How to cite: *Angew. Chem. Int. Ed.* **2021**, *60*, 3417–3421
International Edition: doi.org/10.1002/anie.202015262
German Edition: doi.org/10.1002/ange.202015262

Gas Separation

# Docking of $Cu^I$ and $Ag^I$ in Metal–Organic Frameworks for Adsorption and Separation of Xenon

*Haoze Wang[+], Zhaolin Shi[+], Jingjing Yang[+], Tu Sun, Bunyarat Rungtaweevoranit, Hao Lyu, Yue-Biao Zhang,* and Omar M. Yaghi**

***Abstract:*** *We present a metal docking strategy utilizing the precise spatial arrangement of organic struts as metal chelating sites in a MOF. Pairs of uncoordinated N atoms on adjacent pyrazole dicarboxylate linkers distributed along the rod-shaped Al–O secondary building units in MOF-303 [Al(OH)-($C_5H_2O_4N_2$)] were used to chelate $Cu^I$ and $Ag^I$ with atomic precision and yield the metalated Cu- and Ag-MOF-303 compounds [$(CuCl)_{0.50}Al(OH)(C_5H_2O_4N_2)$ and $(AgNO_3)_{0.49}$-$Al(OH)(C_5H_2O_4N_2)$]. The coordination geometries of $Cu^I$ and $Ag^I$ were examined using 3D electron diffraction and extended X-ray absorption fine structure spectroscopy techniques. The resulting metalated MOFs showed pore sizes matching the size of Xe, thus allowing for binding of Xe from Xe/Kr mixtures with high capacity and selectivity. In particular, Ag-MOF-303 exhibited Xe uptake of 59 $cm^3\,cm^{-3}$ at 298 K and 0.2 bar with a selectivity of 10.4, placing it among the highest performing MOFs.*

Embedding external metal ions into metal–organic frameworks (MOFs)[1] allows access to functional MOFs with enhanced and new properties.[2] Typically, this has been done by anchoring external metal ions on i) secondary building units (SBUs)[3] or ii) organic struts.[4] The latter requires the use of organic struts that bear auxiliary chelating groups such as bipyridyl (Figure 1a),[5] or postsynthetic functionalization of organic struts to introduce chelating sites (Figure 1b).[6] More recently, a molecular vise approach has been demonstrated by partially replacing tetratopic linkers with tritopic linkers to create "defective" binding sites (Figure 1c).[7] Herein, we present a new metalation strategy that utilizes the precise spatial arrangement of organic struts in a MOF to create metal chelating sites (Figure 1d), in a manner reminiscent of metalloenzymes having defined spatial arrangement of multiple binding functionalities.[8] We show that in MOF-303 [$Al(OH)(C_5H_2O_4N_2)$][9] constructed from $Al^{3+}$ and 1*H*-pyrazole-3,5-dicarboxylate (PZDC) linkers, the adjacent pair of uncoordinated N atoms of the pyrazole dicarboxylates along the rod-shaped Al–O SBUs could be used to precisely chelate additional $Cu^I$ and $Ag^I$ to yield the metalated Cu- and Ag-MOF-303 compounds [$(CuCl)_{0.50}Al(OH)(C_5H_2O_4N_2)$ and $(AgNO_3)_{0.49}Al(OH)(C_5H_2O_4N_2)$] with near complete incorporation efficiency (Figure 1e). We reveal their coordination geometry through 3D electron diffraction[10] and extended X-ray absorption fine structure spectroscopy.

The metalated MOFs remain porous, and show reduced pore sizes of 5.5 Å for Cu-MOF-303 and 5.2 Å for Ag-MOF-303, respectively, compared to that of the pristine MOF-303 (8.7 Å). We further show that these two MOFs exhibited high capacity and selectivity for Xe separation. Specifically, Ag-MOF-303 showed a high Xe uptake of 59 $cm^3\,cm^{-3}$ at 298 K and 0.2 bar with a selectivity of 10.4, which are 2.1 and 1.6 times as high as those of pure MOF-303 (28 $cm^3\,cm^{-3}$ and 6.6), respectively, and ranks among the highest MOFs (record performance of 74 $cm^3\,cm^{-3}$ and 16.7 for NJU-Bai7). Furthermore, we show up to 100% improvement of the dynamic separation performance in comparison with that of the pristine MOF-303 for the efficient, steady, and recyclable separation of Xe from Kr.

MOF-303 was synthesized from an aqueous solution of $AlCl_3{\cdot}6H_2O$ and PZDC at 100 °C according to an adapted literature procedure (Section S1 in SI).[9] Its phase purity and crystallinity were confirmed by powder X-ray diffraction (PXRD; Figure S27). Metalation of MOF-303 with $Cu^I$ or $Ag^I$ was accomplished by immersing the pristine crystals in hot acetonitrile solutions (70 °C) of CuCl or $AgNO_3$ for 2 days (Section S1 in SI). Combined PXRD (Figures S28–S32) and scanning electron microscopy (SEM; Figures S15–S16) of these samples revealed retention of crystallinity after metalation, where the scanning electron micrographs indicated a homogenous single crystal morphology.

Metal loading in Cu- and Ag-MOF-303 was determined by inductively coupled plasma–optical emission spectrometry (ICP-OES) and their chemical formulae were evaluated by elemental analysis to be $(CuCl)_{0.50}Al(OH)(C_5H_2O_4N_2)$ and $(AgNO_3)_{0.49}Al(OH)(C_5H_2O_4N_2)$ for Cu- and Ag-MOF-303, respectively (Section S1 in SI). Energy dispersive spectrosco-

[*] H. Wang,[+] Dr. J. Yang,[+] Dr. B. Rungtaweevoranit, H. Lyu, Prof. Dr. O. M. Yaghi
Department of Chemistry, University of California-Berkeley
Berkeley, CA 94720 (USA)
E-mail: yaghi@berkeley.edu
H. Wang,[+] Dr. J. Yang,[+] Dr. B. Rungtaweevoranit, H. Lyu, Prof. Dr. O. M. Yaghi
Kavli Energy NanoSciences Institute
Berkeley, CA 94720 (USA)
Dr. Z. Shi,[+] T. Sun, Prof. Dr. Y.-B. Zhang
School of Physical Science and Technology, ShanghaiTech University
Shanghai, 201210 (China)
E-mail: zhangyb@shanghaitech.edu.cn
Prof. Dr. O. M. Yaghi
Joint UAEU–UC Berkeley Laboratories for Materials Innovations
UAE University
Alain (United Arab Emirates)
[+] These authors contributed equally to this work.
Supporting information and the ORCID identification number(s) for the author(s) of this article can be found under: https://doi.org/10.1002/anie.202015262.

  

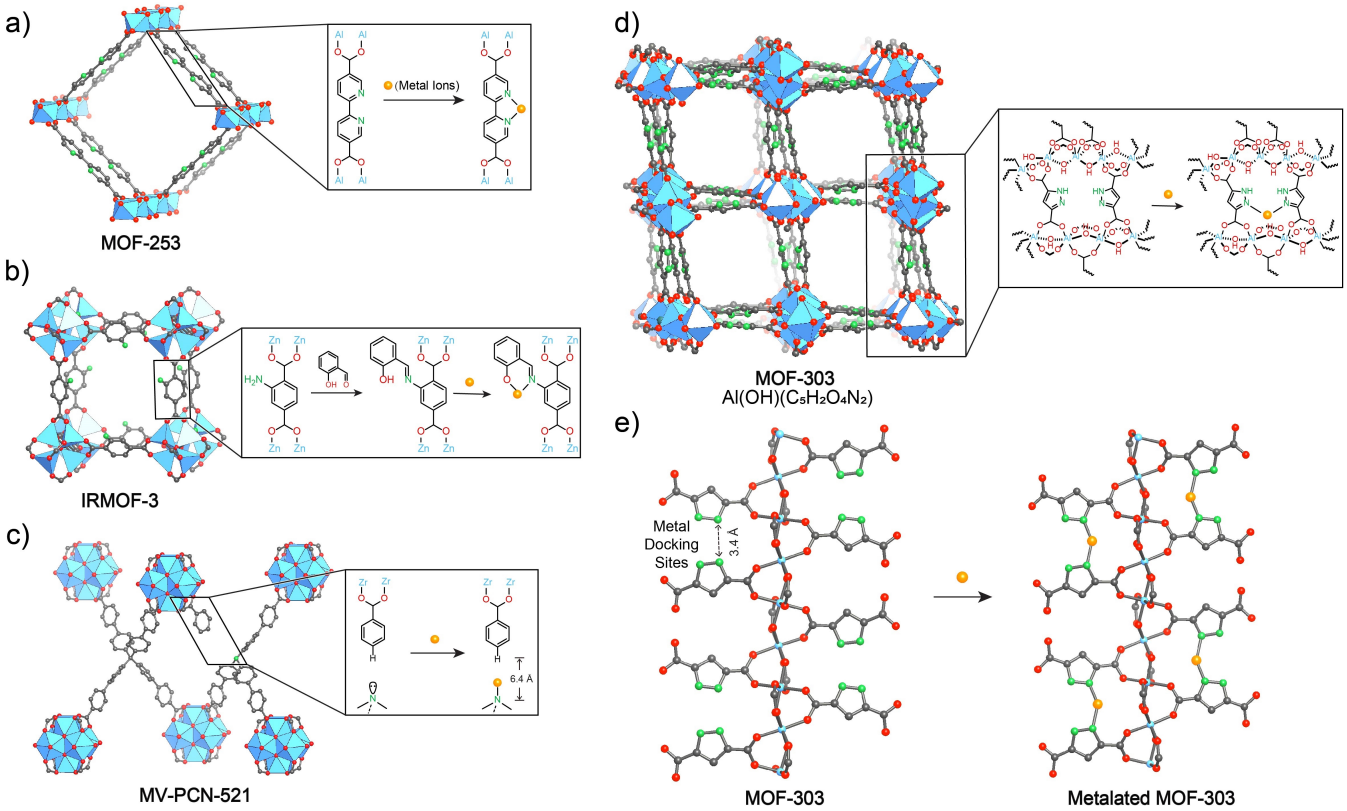


***Figure 1.*** a) Metalation of MOFs on organic struts bearing auxiliary chelating groups, exemplified by introducing additional metal ions to MOF-253 structures. b) Metalation of MOFs on organic struts with postsynthetically introduced chelating sites, illustrated by adding metals to IRMOF-3. c) Metal binding sites generated by the molecular vise approach in MV-PCN-521. d) A new metalation strategy of MOFs by using the spatial arrangement of organic struts as novel metal chelating sites in the MOF matrix, illustrated by adding additional metals to MOF-303. e) Metal docking sites created by pairs of uncoordinated N atoms on adjacent pyrazole dicarboxylate linkers distributed along the rod-shaped one-dimensional Al–O SBUs in MOF-303. Color code: C, gray; O, red; N, green; Zr, Zn, Al, blue; potential additional metal ions, yellow. H atoms are omitted for clarity.

py (EDS) revealed uniform distribution of Cu and Ag ions throughout the MOF crystals (Figures S15–S16).

Structures of the pristine and $Cu^{I}$ and $Ag^{I}$ metalated MOF-303 were determined by 3D electron diffraction tomography (EDT; Figures 2d–f and S17–S22).[11] MOF-303, Cu-, and Ag-MOF-303 crystallized in the monoclinic $P2_1/c$ space group with unit cell parameters of $a=12.3$ Å, $b=15.4$ Å, $c=14.3$ Å, $\alpha=\gamma=90°$, $\beta=101.5°$, $V=2654.3$ Å$^3$; $a=12.7$ Å, $b=15.0$ Å, $c=14.3$ Å, $\beta=102.0°$, $V=2664.6$ Å$^3$; and $a=12.7$ Å, $b=15.5$ Å, $c=14.2$ Å, $\beta=101.7°$, $V=2737.2$ Å$^3$, respectively (Tables S1–S3). In MOF-303, the octahedrally coordinated $Al^{III}$ are bound by four bridging carboxyl groups and two bridging hydroxyl groups to form corner-sharing -Al-O-Al- SBUs. These SBUs are connected by PZDC linkers to give a 3D framework with rhombic channels orientated along the *a*-axis (Figure 1d). The pyrazole rings of two adjacent linkers adopt an edge-to-edge arrangement with N–N distances of 3.4 Å (Figures 1e and 2b), rendering MOF-303 a unique platform to bind additional metal ions. This was confirmed by the crystal structures of Cu- and Ag-MOF-303, in which we observed the chelation of both metal ions by the N atoms of adjacent PZDC linkers. In Cu-MOF-303, the additional $Cu^{I}$ were coordinated by two adjacent PZDC linkers with Cu–N bond lengths of 1.9 Å and 2.1 Å, respectively, resulting in the N–N distances of 3.6 Å (Figure 2a).

The valence of the Cu center and its local coordination sphere were confirmed by the X-ray absorption near edge structure (XANES) and extended X-ray absorption fine structure (EXAFS) spectroscopies, respectively (Section S5 in SI). An absorption peak at 8984 eV corresponding to the $Cu^{I}$ $1s\rightarrow 4p+L$ shakedown transition was observed in the pre-edge region of XANES.[12] A $CuN_2Cl$ core structure was assigned to fit the EXAFS spectrum, which indicated Cu–N and Cu–Cl bond lengths of 1.92 and 2.14 Å, respectively, and is in accordance with the literature.[13] For Ag-MOF-303, we also obtained high-resolution EDT data that showed $Ag^{I}$ ions chelated by two N atoms from adjacent PZDC linkers with Ag–N bond distances of 2.2 and 2.3 Å, respectively (Figure 2c). Compared to the pristine MOF-303, the retained structural symmetry and slightly changed lattice constants of Cu- and Ag-MOF-303 indicated the modularity of MOF-303 as a robust platform for docking additional metal ions.

Porosity of MOF-303, Cu-, and Ag-MOF-303 was examined by their $N_2$ and Ar sorption isotherms. The Brunauer–Emmett–Teller (BET) surface area and pore diameter were measured to be of 1343, 860, and 716 $m^2 g^{-1}$ (Figures S8–S14); 8.7, 5.5 and 5.2 Å, respectively (Figures S4–S7). Reduced

  

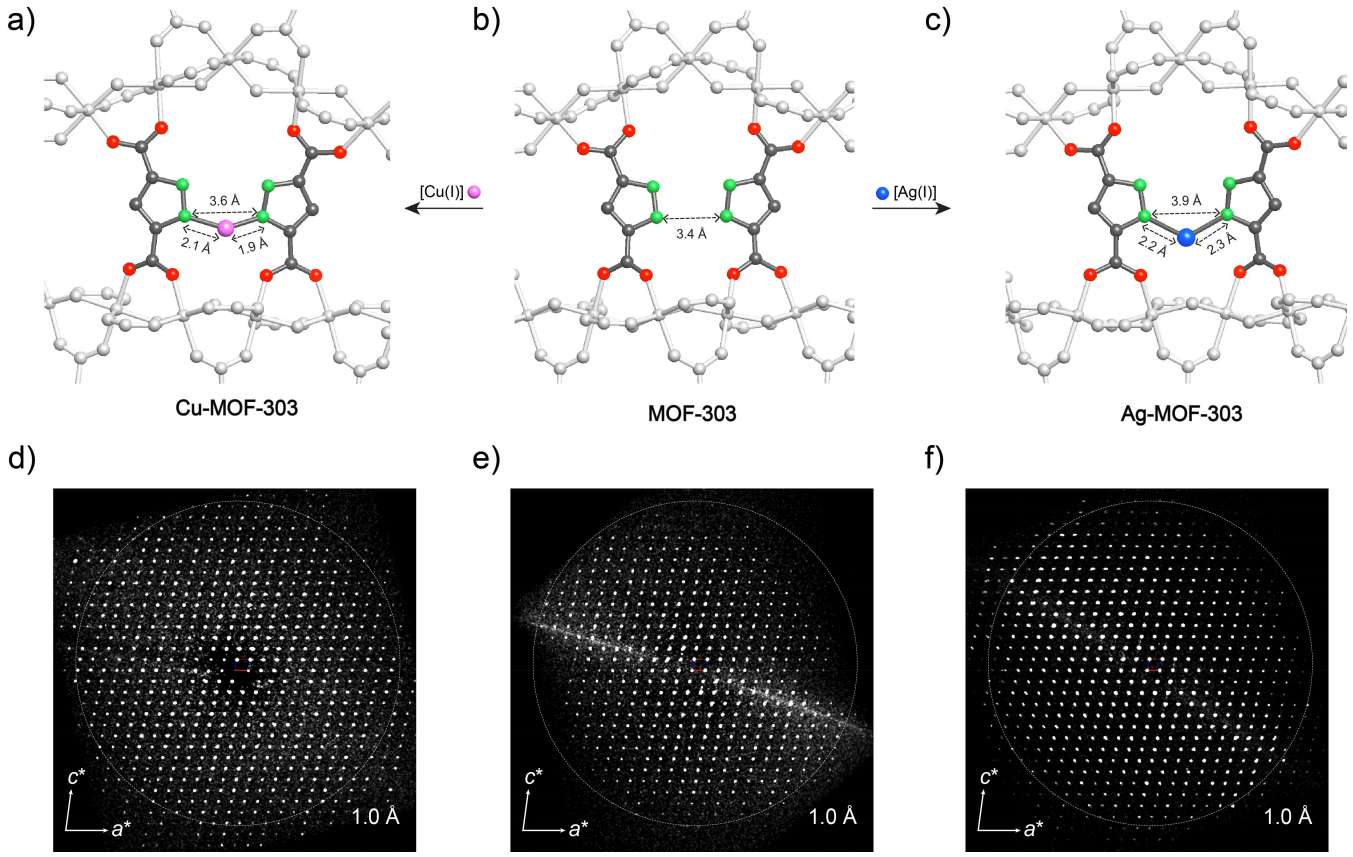


***Figure 2.*** a) Cu-MOF-303 structure as determined from 3D EDT with $Cu^{I}$ ions chelated by N atoms from two adjacent PZDC linkers. b) MOF-303 structure as determined from 3D EDT with pyrazole-based metal docking sites between adjacent PZDC linkers. c) Ag-MOF-303 structure as determined from 3D EDT with $Ag^{I}$ ions chelated by N atoms from two adjacent PZDC linkers. d) Projection of the reconstructed three-dimensional reciprocal lattice of Cu-MOF-303 along the [010] direction. e) Projection of the reconstructed three-dimensional reciprocal lattice of MOF-303 along the [010] direction. f) Projection of the reconstructed three-dimensional reciprocal lattice of Ag-MOF-303 along the [010] direction. Circles represent the resolution of 1.0 Å. Color code: C, gray; O, red; N, green; Cu, pink; Ag, dark blue. H atoms are omitted for clarity.

porosity in metalated Cu- and Ag-MOF-303 arises from the increase of their molecular weights and reduced pore sizes.

To investigate the impact of metalation in MOF-303, we explored their use for Xe/Kr separation. Xe/Kr separation is an industrially important yet energy intensive process.[14] In this context, adsorptive separation by porous zeolites and MOFs[15] is a promising direction compared to traditional cryogenic distillation. Given the larger polarizability of Xe ($40.4\times10^{25}$ cm$^{-3}$) compared to Kr ($24.8\times10^{25}$ cm$^{-3}$),[16] the introduction of polar functional groups (-OH, -$NH_2$, -F, -Cl, -Br, and -I),[17] anions ($CrO_4^{2-}$, $ZrF_6^{2-}$, and $NbOF_5^{2-}$),[18] and metal sites (Co, Ni, Ag, etc.)[19] to polarize Xe for enhanced framework–Xe interactions represents an effective strategy to improve uptake and selectivity of Xe.

We first measured the low-pressure (0–100 kPa) Xe and Kr adsorption isotherms of MOF-303, Cu-, and Ag-MOF-303 at 273, 283, and 298 K, respectively (Figures 3a and S39–S41). Compared to the pristine MOF-303, the Xe uptake capacity at 298 K and 0.2 bar of the Cu- and Ag-MOF-303 were increased from 28 cm$^3$cm$^{-3}$ to 41 cm$^3$cm$^{-3}$ and 59 cm$^3$cm$^{-3}$, respectively (Figure 3e). The Xe/Kr ($v/v=20/80$) selectivity based on the ideal adsorbed solution theory (IAST) was improved from 6.6 to 8.2 and 10.4, respectively (Figures 3c,e). This significant performance improvement in Cu- and Ag-loaded MOF-303 compared to pristine MOF-303 emphasized the importance of metalation. Such high uptake remains consistent throughout 80 cycles of adsorption–desorption experiments (Figure 3d) and ranks among the highest measured for MOFs (record performance of 74 cm$^3$cm$^{-3}$ and 16.7 for NJU-Bai7; Table S5).

The significant improvements in Cu- and Ag-MOF-303 were attributed to the enhanced framework–Xe interactions due to metalation. To probe these interactions, we measured the $^{129}$Xe NMR spectra under isobaric Xe pressures at 293 K in MOF-303, Cu-, and Ag-MOF-303 (Figure S49). The chemical shifts of $^{129}$Xe of MOF-303, Cu-, and Ag-MOF-303 appeared at 93.68, 103.53, and 105.50 ppm, respectively. This trend in downfield shifts indicates greater electron deshielding effects in metalated MOF-303, and thus suggested stronger framework–Xe interactions. This result is also in line with the calculated $Q_{st}$ for the three compounds (23.7, 24.4, and 28.2 kJ mol$^{-1}$, respectively, Figure 3b). The broader linewidths (full width at half maximum, FWHM) of Cu-MOF-303 (11.60 ppm) and Ag-MOF-303 (11.89 ppm) can be attributed to the more heterogeneous pore environments in comparison with pristine MOF-303 (5.79 ppm).

To examine the practical performance of metalated MOFs for extracting Xe from Xe/Kr mixtures, we conducted fixed-

  

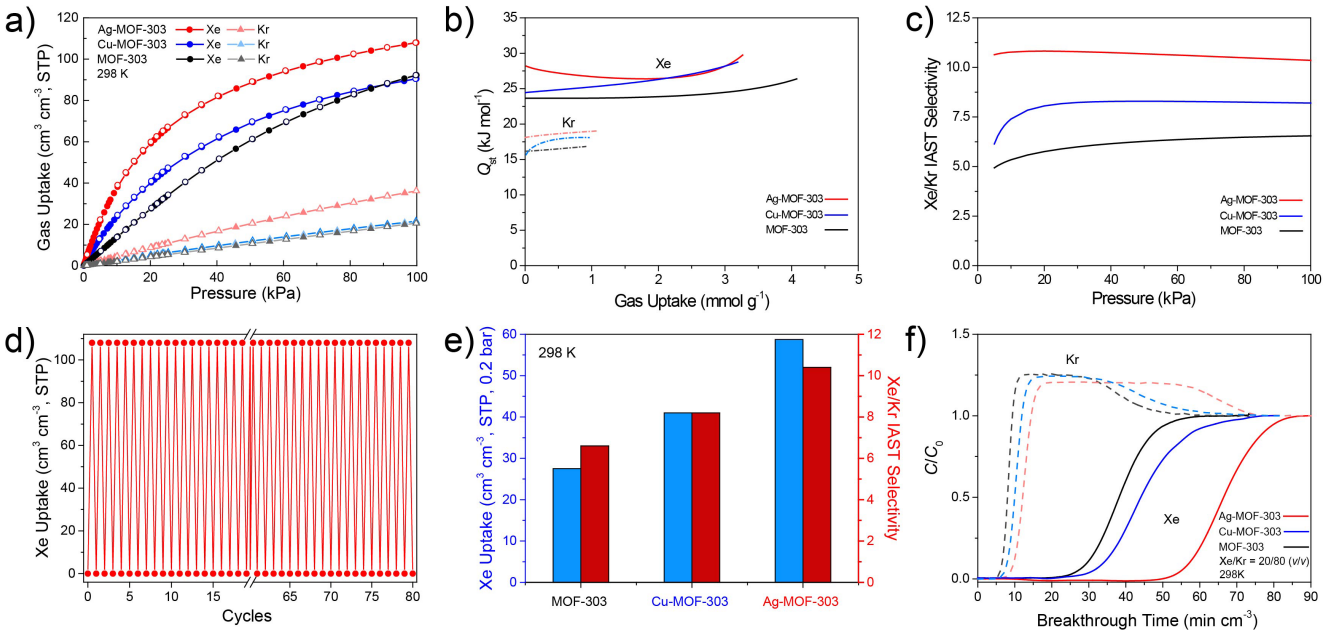


***Figure 3.*** a) Xe and Kr sorption isotherms for MOF-303, Cu-, and Ag-MOF-303 measured at 298 K. Filled and open circles represent adsorption and desorption data, respectively. b) Isosteric heat of adsorption ($Q_{st}$) for Xe/Kr of MOF-303, Cu-, and Ag-MOF-303. c) Calculated IAST selectivity at 298 K for a 20/80 Xe/Kr mixture in MOF-303, Cu-, and Ag-MOF-303 to be 6.6, 8.2, and 10.4, respectively. d) Xe adsorption–desorption cycling data represented by volumetric uptake for Ag-MOF-303 measured at 298 K. Adsorption–desorption cycling measurements were conducted without additional activation of Ag-MOF-303; between the cycles the sample was regenerated by evacuation at 298 K, demonstrating mild regeneration conditions and cyclic stability of 80 Xe adsorption cycles. e) Comparison of Xe separation performance between MOF-303, Cu-, and Ag-MOF-303. Metalation of MOFs showed significant improvement in Xe uptake capacity and Xe/Kr selectivity. f) Experimental breakthrough curves for a binary Xe/Kr mixture [20/80 (v/v)] at 298 K and 1.1 bar showing the separation performance of MOF-303, Cu-, and Ag-MOF-303. STP: standard temperature and pressure. Solid and dashed lines refer to Xe and Kr, respectively.

bed breakthrough experiments with a representative inlet gas mixture [Xe/Kr = 20/80 (*v/v*)]. A 540 mg sample of Ag-MOF-303 was packed in a column through which the Xe/Kr mixture passed through (Scheme S1). As shown in Figure 3 f, the Ag-MOF-303 bed held at capacities of Xe of 3000 $scm^{-3}$ and capacities of Kr of 600 $scm^{-3}$. The large difference in the breakthrough time between Xe and Kr confirmed the performance of Ag-MOF-303 in Xe/Kr separations. In comparison with the pristine MOF-303, Cu- and Ag-MOF-303 exhibited greatly enhanced separation performance for Xe/Kr, with an improved retention time for Xe by 100% in Ag-MOF-303. The metalated MOF-303 could easily be regenerated by purging an inert Ar flow, after which the dynamic adsorption capacity remained unchanged throughout the measurements (65 cycles; Figure S48).

In summary, we presented a unique metal docking strategy in MOFs that makes use of the precise spatial arrangement of organic linkers distributed along a rod-shaped SBU as metal chelating sites. This approach uses simple organic linkers, does not require the installation of additional binding sites, and gives access to metalated MOF-303 with high Xe capacity and separation performance.

## Acknowledgements

We appreciate the continued support and interest of KACST (Center of Excellence for Nanomaterials and Clean Energy Applications). Preliminary characterization of compounds was supported in part by Berkeley Global Science Institute and UAEU. The NMR facility in College of Chemistry is supported in part by NIH S10OD024998. Gas adsorption and separation were conducted at the Analytical Instrumentation Center (#SPST-AIC 10112914), and electron diffraction tomography were conducted at the C*ħ*EM (#EM02161943), SPST, ShanghaiTech University. We thank Prof. W. Wang and Z. Wang at Lanzhou University for acquisition of $^{129}$Xe NMR spectra, Dr. S. Fakra for analysis of X-ray absorption spectroscopy. We also thank Prof. Y. Ma, Dr. Y. Liu, Dr. C. S. Diercks, Dr. Z. Ji, Dr. C. Gropp, and Dr. B. Zhang for beneficial discussion.

## Conflict of interest

The authors declare no conflict of interest.

**Keywords:** copper · silver · metal docking · metal–organic frameworks · xenon separation

[1] O. M. Yaghi, M. J. Kalmutzki, C. S. Diercks, *Introduction to Reticular Chemistry: Metal-Organic Frameworks and Covalent Organic Frameworks*, Wiley-VCH, Weinheim, **2019**.

[2] a) K. L. Mulfort, O. K. Farha, C. L. Stern, A. A. Sarjeant, J. T. Hupp, *J. Am. Chem. Soc.* **2009**, *131*, 3866–3868; b) L. Ma, J. M. Falkowski, C. Abney, W. Lin, *Nat. Chem.* **2010**, *2*, 838–847;

  

c) M. H. Beyzavi, N. A. Vermeulen, A. J. Howarth, S. Tussupbayev, A. B. League, N. M. Schweitzer, J. Hupp, O. K. Farha, *J. Am. Chem. Soc.* **2015**, *137*, 13624 – 13631; d) J. Baek, B. Rungtaweevoranit, X. Pei, M. Park, S. C. Fakra, Y. Liu, R. Matheu, S. A. Alshmimri, S. Alshehri, C. A. Trickett, G. A. Somorjai, O. M. Yaghi, *J. Am. Chem. Soc.* **2018**, *140*, 18208 – 18216; e) W. Pi, X. Feng, Y. Song, Z. Xu, Z. Li, W. Lin, *J. Am. Chem. Soc.* **2020**, *142*, 10302 – 10307; f) R. A. Peralta, M. T. Huxley, J. D. Evans, T. Fallon, H. Cao, M. He, X. Zhao, S. Agnoli, C. J. Sumby, C. J. Doonan, *J. Am. Chem. Soc.* **2020**, *142*, 13533 – 13543.

[3] a) J. E. Mondloch, W. Bury, D. Fairen-Jimenez, S. Kwon, E. J. DeMarco, M. H. Weston, A. A. Sarjeant, S. T. Nguyen, P. C. Stair, R. Q. Snurr, O. K. Farha, J. T. Hupp, *J. Am. Chem. Soc.* **2013**, *135*, 10294 – 10297; b) S. Yuan, Y. P. Chen, J. Qin, W. Lu, X. Wang, Q. Zhang, H. C. Zhou, *Angew. Chem. Int. Ed.* **2015**, *54*, 14696 – 14700; *Angew. Chem.* **2015**, *127*, 14909 – 14913; c) I. S. Kim, J. Borycz, A. E. Platero-Prats, S. Tussupbayev, T. C. Wang, O. K. Farha, J. T. Hupp, L. Gagliardi, K. W. Chapman, C. J. Cramer, A. B. F. Martinson, *Chem. Mater.* **2015**, *27*, 4772 – 4778; d) Z. Li, N. M. Schweitzer, A. B. League, V. Bernales, A. W. Peters, A. B. Getsoian, T. C. Wang, J. T. Miller, A. Vjunov, J. L. Fulton, J. A. Lercher, C. J. Cramer, L. Gagliardi, J. T. Hupp, O. K. Farha, *J. Am. Chem. Soc.* **2016**, *138*, 1977 – 1982; e) A. M. Abdel-Mageed, B. Rungtaweevoranit, M. Parlinska-Wojtan, X. Pei, O. M. Yaghi, R. J. Behm, *J. Am. Chem. Soc.* **2019**, *141*, 5201 – 5210.

[4] J. D. Evans, C. J. Sumby, C. J. Doonan, *Chem. Soc. Rev.* **2014**, *43*, 5933 – 5951.

[5] a) E. D. Bloch, D. Britt, C. J. Doonan, F. J. Uribe-Romo, H. Furukawa, J. R. Long, O. M. Yaghi, *J. Am. Chem. Soc.* **2010**, *132*, 14382 – 14384; b) A. M. Shultz, A. A. Sarjeant, O. K. Farha, J. T. Hupp, S. T. Nguyen, *J. Am. Chem. Soc.* **2011**, *133*, 13252 – 13255; c) W. Morris, B. Volosskiy, S. Demir, F. Gándara, P. L. McGrier, H. Furukawa, D. Cascio, J. F. Stoddart, O. M. Yaghi, *Inorg. Chem.* **2012**, *51*, 6443 – 6445; d) W. M. Bloch, A. Burgun, C. J. Coghlan, R. Lee, M. L. Coote, C. J. Doonan, C. J. Sumby, *Nat. Chem.* **2014**, *6*, 906 – 912; e) K. Manna, T. Zhang, W. Lin, *J. Am. Chem. Soc.* **2014**, *136*, 6566 – 6569; f) H. Fei, S. M. Cohen, *J. Am. Chem. Soc.* **2015**, *137*, 2191 – 2194.

[6] a) M. J. Ingleson, J. P. Barrio, J.-B. Guilbaud, Y. Z. Khimyak, M. J. Rosseinsky, *Chem. Commun.* **2008**, 2680 – 2682; b) C. J. Doonan, W. Morris, H. Furukawa, O. M. Yaghi, *J. Am. Chem. Soc.* **2009**, *131*, 9492 – 9493; c) K. K. Tanabe, S. M. Cohen, *Angew. Chem. Int. Ed.* **2009**, *48*, 7424 – 7427; *Angew. Chem.* **2009**, *121*, 7560 – 7563; d) T. Gadzikwa, O. K. Farha, K. L. Mulfort, J. T. Hupp, S. T. Nguyen, *Chem. Commun.* **2009**, 3720 – 3722.

[7] a) Y. Wang, Q. Liu, Q. Zhang, B. Peng, H. Deng, *Angew. Chem. Int. Ed.* **2018**, *57*, 7120 – 7125; *Angew. Chem.* **2018**, *130*, 7238 – 7243; b) W. Yan, S. Li, T. Yang, Y. Xia, X. Zhang, C. Wang, Z. Yan, F. Deng, Q. Zhou, H. Deng, *J. Am. Chem. Soc.* **2020**, *142*, 16182 – 16187.

[8] K. D. Karlin, *Science* **1993**, *261*, 701 – 708.

[9] a) F. Fathieh, M. J. Kalmutzki, E. A. Kapustin, P. J. Waller, J. Yang, O. M. Yaghi, *Sci. Adv.* **2018**, *4*, eaat3198; b) N. Hanikel, M. S. Prévot, F. Fathieh, E. A. Kapustin, H. Lyu, H. Wang, N. J. Diercks, T. G. Glover, O. M. Yaghi, *ACS Cent. Sci.* **2019**, *5*, 1699 – 1706.

[10] a) U. Kolb, T. Gorelik, C. Kübel, M. T. Otten, D. Hubert, *Ultramicroscopy* **2007**, *107*, 507 – 513; b) D. Zhang, P. Oleynikov, S. Hovmöller, X. Zou, *Z. Kristallogr.* **2010**, *225*, 94 – 102; c) "Electron Diffraction": H. Lu, K. Miyasaka, O. Terasaki, in *Structure from Diffraction Methods* (Eds.: D. W. Bruce, D. O'Hare, R. I. Walton), Wiley, Hoboken, **2014**, pp. 216 – 229; d) Z. Huang, E. S. Grape, J. Li, A. K. Inge, X. Zou, *Coord. Chem. Rev.* **2021**, *427*, 213583.

[11] a) T. Sun, L. Wei, Y. Chen, Y. Ma, Y.-B. Zhang, *J. Am. Chem. Soc.* **2019**, *141*, 10962 – 10966; b) T. Sun, W. Lei, Y. Ma, Y.-B. Zhang, *Chin. J. Chem.* **2020**, *38*, 1153 – 1166.

[12] L.-S. Kau, D. J. Spira-Solomon, J. E. Penner-Hahn, K. O. Hodgson, E. I. Solomon, *J. Am. Chem. Soc.* **1987**, *109*, 6433 – 6442.

[13] a) A.-X. Zhu, Q.-Q. Xu, F.-Y. Liu, Z. Li, X.-L. Qi, *Inorg. Chim. Acta* **2011**, *370*, 333 – 339; b) Y. Chen, L. Li, Y. Cao, J. Wu, Q. Cao, Y. Li, H. Hu, W. Liu, Y. Liu, Z. Kang, J. Li, *CrystEngComm* **2013**, *15*, 2675 – 2681; c) A. Beheshtia, E. S. Mousavifarda, S. Noorizadeha, P. Mayerb, K. Woźniak, *Inorg. Chim. Acta* **2019**, *497*, 119082.

[14] a) F. G. Kerry, *Industrial Gas Handbook: Gas Separation and Purification*, CRC Press, Boca Raton, FL, **2007**; b) D. Banerjee, A. J. Cairns, J. Liu, R. K. Motkuri, S. K. Nune, C. A. Fernandez, R. Krishna, D. M. Strachan, P. K. Thallapally, *Acc. Chem. Res.* **2015**, *48*, 211 – 219.

[15] a) C. Gücüyener, J. van den Bergh, J. Gascon, F. Kapteijn, *J. Am. Chem. Soc.* **2010**, *132*, 17704 – 17706; b) E. D. Bloch, W. L. Queen, R. Krishna, J. M. Zadrozny, C. M. Brown, J. R. Long, *Science* **2012**, *335*, 1606 – 1610; c) A. Cadiau, K. Adil, P. M. Bhatt, Y. Belmabkhout, M. Eddaoudi, *Science* **2016**, *353*, 137 – 140; d) L. Li, R.-B. Lin, R. Krishna, H. Li, S. Xiang, H. Wu, J. Li, W. Zhou, B. Chen, *Science* **2018**, *362*, 443 – 446; e) D. Banerjee, C. M. Simon, S. K. Elsaidi, M. Haranczyk, P. K. Thallapally, *Chem* **2018**, *4*, 466 – 494; f) R. Lin, S. Xiang, W. Zhou, B. Chen, *Chem* **2020**, *6*, 337 – 363.

[16] J. R. Li, R. J. Kuppler, H. C. Zhou, *Chem. Soc. Rev.* **2009**, *38*, 1477 – 1504.

[17] a) S. T. Meek, S. L. Teich-McGoldrick, J. J. Perry, J. A. Greathouse, M. D. Allendorf, *J. Phys. Chem. C* **2012**, *116*, 19765 – 19772; b) X. Chen, A. M. Plonka, D. Banerjee, R. Krishna, H. T. Schaef, S. Ghose, P. K. Thallapally, J. B. Parise, *J. Am. Chem. Soc.* **2015**, *137*, 7007 – 7010; c) S.-J. Lee, S. Kim, E.-J. Kim, M. Kim, Y.-S. Bae, *Chem. Eng. J.* **2018**, *335*, 345 – 351; d) L. Li, L. Guo, Z. Zhang, Q. Yang, Y. Yang, Z. Bao, Q. Ren, J. Li, *J. Am. Chem. Soc.* **2019**, *141*, 9358 – 9364.

[18] a) M. H. Mohamed, S. K. Elsaidi, T. Pham, K. A. Forrest, H. T. Schaef, A. Hogan, L. Wojtas, W. Xu, B. Space, M. J. Zaworotko, P. K. Thallapally, *Angew. Chem. Int. Ed.* **2016**, *55*, 8285 – 8289; *Angew. Chem.* **2016**, *128*, 8425 – 8429; b) S. K. Elsaidi, M. H. Mohamed, C. M. Simon, E. Braun, T. Pham, K. A. Forrest, W. Xu, D. Banerjee, B. Space, M. J. Zaworotko, P. K. Thallapally, *Chem. Sci.* **2017**, *8*, 2373 – 2380; c) Q. Wang, T. Ke, L. Yang, Z. Zhang, X. Cui, Z. Bao, Q. Ren, Q. Yang, H. Xing, *Angew. Chem. Int. Ed.* **2020**, *59*, 3423 – 3428; *Angew. Chem.* **2020**, *132*, 3451 – 3456.

[19] a) S. M. Kuznicki, A. Ansón, A. Koenig, T. M. Kuznicki, T. Haastrup, E. M. Eyring, D. Hunter, *J. Phys. Chem. C* **2007**, *111*, 1560 – 1562; b) C. Daniel, A. Elbaraoui, S. Aguado, M.-A. Springuel-Huet, A. Nossov, J.-P. Fontaine, S. Topin, T. Taffary, L. Deliere, Y. Schuurman, D. Farrusseng, *J. Phys. Chem. C* **2013**, *117*, 15122 – 15129; c) J. J. Perry, S. L. Teich-McGoldrick, S. T. Meek, J. A. Greathouse, M. Haranczyk, M. D. Allendorf, *J. Phys. Chem. C* **2014**, *118*, 11685 – 11698; d) M. T. Kapelewski, J. Oktawiec, T. Runčevski, M. I. Gonzalez, J. R. Long, *Isr. J. Chem.* **2018**, *58*, 1138 – 1143; e) Y. Wang, W. Liu, Z. Bai, T. Zheng, M. A. Silver, Y. Li, Y. Wang, X. Wang, J. Diwu, Z. Chai, S. Wang, *Angew. Chem. Int. Ed.* **2018**, *57*, 5783 – 5787; *Angew. Chem.* **2018**, *130*, 5885 – 5889.

Manuscript received: November 16, 2020
Accepted manuscript online: November 27, 2020
Version of record online: January 26, 2021

  